Proceedings of IMECE'03:
2003 ASME International Mechanical Engineering Congress & Exposition
Washington, D.C., November 16-21, 2003

IMECE2003-41945

DESIGN OF RADIO FREQUENCY (RF) MEMS SWITCHES – MODELING

Yong Zhu and Horacio D. Espinosa

Department of Mechanical Engineering, Northwestern University, Evanston, IL 60208-3111, USA
Tel: (847)467-5989, Fax: (847)491-3915, Email: espinosa@northwestern.edu

ABSTRACT

Mechanical modeling of RF MEMS switches is important for performance optimization and device reliability. 1-D, 2-D, and 3-D linear analytical models have been proposed to analyze the electrostatic pull-in of a fixed-fixed beam at small deflection. However, most RF MEMS switch structures work at large deflection range. In this paper, 1-D, 2-D, and 3-D nonlinear analytical models suitable for large structural deflection are developed in a generalized form. In some practical applications, finite element models are required to account for the effects of all the design parameters: switch geometry, non-uniform state of residual stress, temperature and etc. A 3-D finite element model between structural, electrical and thermal domains is developed. This 3-D model is applicable to the design of all types of electrostatic actuators, though that of a capacitive coupling switch was examined.

1. INTRODUCTION

Microelectromechanical Systems (MEMS) for radio frequency (RF) applications or RF MEMS provides an opportunity to revolutionize the wireless communication. Modeling of RF MEMS devices is essential for design optimization and device reliability. One of the most important RF MEMS components is MEMS switch.

The design of a MEMS switch involves the knowledge of several disciplines: mechanics, electronics, and material science. An ideal switch ought to have high isolation, low insertion loss, low power consumption and high reliability [1]. The first two aspects are directly related to electrical engineering. However, power consumption and reliability are two areas in which mechanical engineers are poised to contribute through optimal structural design.

Modeling of MEMS switches becomes more complicated at some applications where low temperatures are expected, e.g., aircraft condition monitoring [2] and satellite communication [3]. The switch geometry and residual stress state are functions of operational temperature.

In this paper, various analytical models are discussed followed by a Finite Element Analysis (FEA) model involving structural, electrical and thermal domains. As a case study, this model is applied to a capacitive coupling MEMS switch.

2. ANALYTICAL MODELS OF MEMS SWITCHES

2.1. Electromechanical Analysis of MEMS Switches

For the structure and operation of RF MEMS switches, please see [4-5] for details. Fig. 1 presents the schematic of a capacitive coupling MEMS switch.

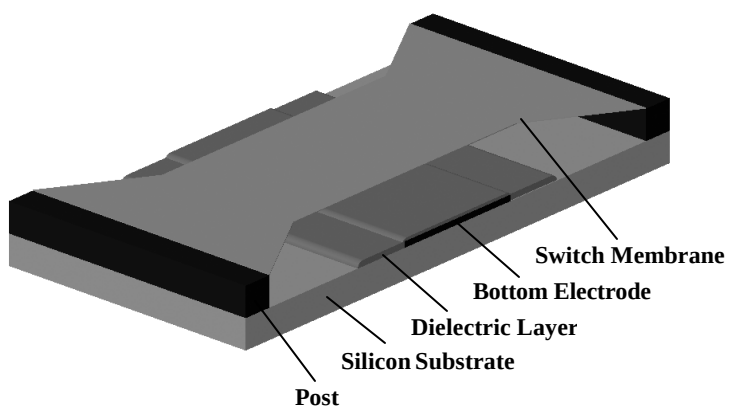

Fig. 1. Shematic of a capacitive coupling MEMS switch

Given the potentials on the electrodes, the potential distribution is calculated by an electrostatic analysis. The problem can be described by *Laplace*'s equation with two known potential boundary conditions, namely,

$$\nabla^2 V = \frac{\partial^2 V}{\partial x^2} + \frac{\partial^2 V}{\partial y^2} + \frac{\partial^2 V}{\partial z^2} = 0 \qquad (1.1)$$

$$V = V_0 \quad \text{at switch membrane (top electrode)} \qquad (1.2)$$

$$V = 0 \qquad \text{at bottom electrode} \tag{1.3}$$

where V denotes the potential distribution in the medium (such as air and vacuum) surrounding the two electrodes, and V_0 is the applied voltage on the top electrode. This equation is suitable to any configuration of the switch, not necessary to be flat. For a point of the switch membrane deflected by $w(x, y)$ and after the potential distribution in the medium is obtained, a unique electrostatic field is determined from the following equations:

$$\boldsymbol{E} = -\nabla V \tag{2.1}$$

$$r_S = eE_N \tag{2.2}$$

$$\boldsymbol{P} = \frac{1}{2} r_S \boldsymbol{E} \tag{2.3}$$

where $\boldsymbol{E}$ is the electric field, E_N is the magnitude of electric field normal to the membrane surface, e is the electric permittivity of the surrounding medium, r_S is the surface charge density, and $\boldsymbol{P}$ is the pressure on the electrodes. In short, the solution of the electrostatic problem can be represented as:

$$\boldsymbol{P} = \boldsymbol{S}_E(w, V_0) \tag{3}$$

where $\boldsymbol{S}_E(w, V_0)$ denotes the solution for the electrostatic pressure $\boldsymbol{P}$ on the membrane, given the membrane deflection w and the applied voltage V_0 between the top and bottom electrodes.

After obtaining the electrostatic pressure, the next task is to find the corresponding deflection of the switch membrane, which is usually more complicated than its electrostatic counterpart. In general, the switch membrane deflection is a function of electrostatic pressure,

$$w = S_S(\boldsymbol{P}) \tag{4}$$

where $S_S(\boldsymbol{P})$ is the solution of the structural displacement, w, given the electrostatic pressure $\boldsymbol{P}$.

3-D coupled field solver including structural, electrostatic and thermal analyses is required to obtain the deflection. However, this comprehensive solver is not efficient in CPU time and may present convergence difficulties. In some practical cases, we are able to use some simplified analytical models to describe the deflection of the switch membrane. In the following sections, we will discuss the 1-D parallel-plate actuator model, the 2-D distributed model, and the 3-D distributed model. [9-16].

2.2. The 1-D Parallel-Plate Actuator Model

One important device characteristic for a MEMS switch is the actuation voltage, which is determined primarily by the mechanical stiffness of the switch membrane and the gap between the top and bottom electrodes. The membrane stiffness is related to the membrane geometry (in-plane shape and out-of-plane profile), material properties and residual stress state. A first-order approximation of this device is a system consisting of two parallel conductive plates separated by gap g_0, with one plate fixed on the substrate and the other suspended by a linear spring. When a voltage V is applied across the plates, the force balance equation, which includes the electrostatic force and the spring restoring force is given by

$$\frac{eAV^2}{2(g_0 - w)^2} - K_{eff} w = 0 \tag{5}$$

where $K_{eff} = \frac{32Ebt^3}{L^3} + \frac{8T}{L}$ is the effective structural stiffness, $T = s_0(1-n)bt$, A is the area of the movable plate, g_0 is the initial gap, w is the deflection, E is the Young's modulus, t is the plate thickness, s_0 is the biaxial residual stress presumed present before the plate shape is etched [6], and n is the Poisson's ratio.

As V increases, the movable plate is deflected down gradually. However, at pull-in voltage or actuation voltage, $V_{pull-in} = \sqrt{\frac{8k_{eff}}{27eA} g_0^3}$, the system becomes unstable and the plate suddenly collapses. The corresponding gap is $2/3 g_0$.

This linear spring approximation is valid for the small deflection of the switch membrane. Here small deflection means the deflection is comparably smaller than the membrane thickness. However, for a capacitive MEMS switch the deflection is usually on the order of its thickness. Hence, to describe the switch membrane deflection, the Duffing spring with a nonlinear term should be used instead [7]. Then the force balance equation becomes

$$\frac{eAV^2}{2(g_0 - w)^2} - k_1 w - k_3 w^3 = 0 \tag{6}$$

where $K_1 = \frac{32Ebt^3}{L^3} + \frac{8T}{L^2}$ and $k_3 = \frac{p^4 Ebt}{8L^3}$ [3]. The first order term in the Duffing spring arises from the switch membrane bending and residual stress, and the third order term originates from the strain stiffening effect. As the switch membrane deflects, the tensile stress in the membrane increases due to in-plane strain (a form of geometric nonlinearity). This tensile stress increases the membrane stiffness. At large deflection, the strain stiffening effect can become dominant.

Not only do the effects of strain stiffening increase the pull-in voltage, but also increase the deflection range before pull-in. In general, the spring restoring force and the gap at pull-in instability are related as

$$F_m = kw^a \tag{7.1}$$

$$g_{pull-in} = \frac{2}{2+a} g_0 \tag{7.2}$$

where a is an index factor representing the constitutive relation (e.g., 1, 2, 3).

When $a = 1$ (at small deflection where bending and residual stress are dominant), the gap at pull-in is 2/3 of the initial gap, which is the case of the linear spring parallel-plate actuator. By contrast, when $a = 3$ (at large deflection where the strain stiffening effect is dominant), the gap at pull-in is 2/5 of the initial gap. For a real device, the pull-in gap lies between $\frac{2}{3}g_0$ and $\frac{2}{5}g_0$ depending on the device geometry and residual stress. As a matter of fact, Hung and Senturia took advantage of this large motion before pull-in instability to extend the travel range of electrostatic actuators [7].

2.3. The 2-D Distributed Beam Model

Since the deflection along the switch membrane is not uniform, the electrostatic field is accordingly position dependent rather than uniform as assumed in the 1-D model. Switch membrane should be modeled as a plate since its width is comparable to its length. However, for a rectangular-shaped switch, a cross section of the switch membrane is considered as a beam under the assumption of plane strain. The Ordinary Differential Equation (ODE) describing the beam deflection under distributed electrostatic force is given by

$$\tilde{E}I\frac{d^4w}{dx^4} = -\frac{ebV^2}{2(g_0 - w)^2} + T(\frac{d^2w}{dx^2}) \tag{8}$$

where $\tilde{E} = \frac{E}{1-n^2}$ is the plate modulus, $I = \frac{1}{12}bt^3$ is the moment of inertia with respect to the length direction (x-direction), and b is the plate width. The fringing field is neglected for the capacitive switch, since its gap is much smaller than its side length.

Eq. (8) is a linear distributed model and only valid for small deflection. At large deflection, the equation describing large beam deflection is

$$\tilde{E}I\frac{d^4w}{dx^4} = -\frac{ebV_0^2}{2(g_0 - w)^2} + \frac{Ebt}{2(1-n^2)}(\frac{dw}{dx})^2(\frac{d^2w}{dx^2}) + T(\frac{d^2w}{dx^2}) \tag{9}$$

where the first term on the right arises from electrostatic force, the second term originates from nonlinear kinematics, and the third term derives from residual stress. Eqs. [8] and [9] are simplified versions of plate model, which is discussed in the following.

2.4. The 3-D Distributed Plate Model

If the switch membrane is not rectangular or circular, it is inaccurate to assume plane strain and use 2-D beam model. Rather, 3-D distributed plate model should be used. The Partial Differential Equation (PDE) describing the plate deflection is given by

$$\nabla^4 w = \frac{1}{D}[\frac{eV_0^2}{2(g_0 - w)^2} + s_0 t(\frac{\partial^2 w}{\partial x^2}) + s_0 t(\frac{\partial^2 w}{\partial y^2})] \tag{10}$$

where $\nabla^4() \equiv \frac{\partial^4}{\partial x^4} + \frac{\partial^4}{\partial x^2 \partial y^2} + \frac{\partial^4}{\partial y^4}$.

The in-plane strains due to large deflection are

$$e_x = \frac{1}{2}[\frac{\partial w(x,y)}{\partial y}]^2 \tag{11.1}$$

$$e_y = \frac{1}{2}[\frac{\partial w(x,y)}{\partial x}]^2 \tag{11.2}$$

$$w = \frac{\partial w(x,y)}{\partial x}\frac{\partial w(x,y)}{\partial y} \tag{11.3}$$

where e_x and e_y are normal strains and w is shear strain. As a result, the large deflection is described by [8]

$$\nabla^4 w = \frac{1}{D}[\frac{eV_0^2}{2(g_0 - w)^2} + \frac{Et}{1-n^2}(e_x + ne_y)(\frac{\partial^2 w}{\partial x^2}) + \frac{Et}{1-n^2}(e_y + ne_x)(\frac{\partial^2 w}{\partial y^2}) - \frac{Et}{1+n}w(\frac{\partial^2 w}{\partial x \partial y}) + s_0 t((\frac{\partial^2 w}{\partial x^2}) + (\frac{\partial^2 w}{\partial y^2}))] \tag{12}$$

Up to now, the analytical models covering both small and large deflections are complete. Both ODEs and PDEs can be solved by relaxation method [9] though it is difficult for nonlinear PDEs. 3-D plate model can describe the case of various in-plane shapes and even nonuniform residual stress. Nevertheless, an out-of-plane profile is typically present in the MEMS switch. What's more, when operational temperature varies, the switch geometry and residual stress vary accordingly, which makes the problem even more complicated. In this case, a coupled field FEA model including structural, electrostatic and thermal domains is required.

3. DEVELOPMENT OF THE FEA MODEL

The model was developed using ANSYS/Multiphysics, see [10] for details. The simulation consisted of two steps in sequence: thermal-structural analysis and electrostatic-structural analysis. If the temperature is constant, only second step, electrostatic-structural analysis, is needed. Two physical environments, electrostatic and structural environments, were defined based on the solid model and boundary conditions.

First the thermo-mechanical analysis was performed within the structural environment. A uniform temperature was applied to the device and the thermal expansion coefficient used for the membrane was assumed to be the difference between that for the membrane and the substrate. The thermo-mechanical analysis resulted in a new switch geometry, especially its out-of-plane profile, and in-plane thermal stresses. This new geometry and new stress state was used as the starting point for the subsequent electrostatic-structural analysis.

The electrostatic-structural analysis was performed as a sequentially coupled analysis involving a two-way coupling between both the electrostatic and structural environments. In the electrostatic environment, the voltage distribution in the surrounding medium was obtained and the electrostatic force

between the two conductors was calculated. Then, the analysis environment was switched to the structural environment. A new deformation state was obtained arising from the electrostatic force. The analysis was switched back to the electrostatic environment and the electrostatic mesh was updated according to the updated membrane geometry. Iterations between these two physical environments were executed in sequence until convergence in both environments was reached. This process was repeated for every applied voltage until pull-in happens.

Shell elements were employed to model the switch membrane and solid elements were used to model the surrounding medium to account for the electrostatic field. The boundary conditions used in the mechanical analysis were fixed-fixed at both ends of the freestanding membrane. For the electrostatic analysis, Equations (1.2) and (1.3) were employed as boundary conditions. This FEA model is suitable to the static analysis of all types of electrostatic actuators at various operational temperatures.

Fig. 2 compares 1-D and 2-D analytical models and 3-D FEA model for a rectangular switch membrane. At small deflection, all the models present close results. However, at large deflection, linear models exhibit big error. The 2-D nonlinear model shows a good match to the 3-D FEA simulation. 1-D nonlinear model gives an approximate prediction of the pull-in gap.

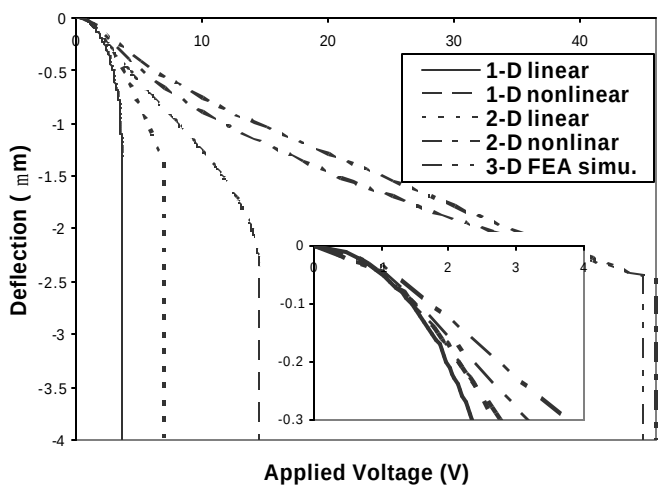

Fig. 2. Comparison of various models for a rectangular switch (L=320 μm, b=100 μm and t=0.3 μm). Inset shows applied voltage-deflection curves at small deflection.

4. CASE STUDY: CAPACITIVE COUPLING SWITCH

In this section, we discuss the effects of residual stress, switch geometry, and temperature on the actuation voltage of a bow tie capacitive coupling switch. The model does not include the etching holes, as shown in Fig. 3. For the effect of holes, see [11].

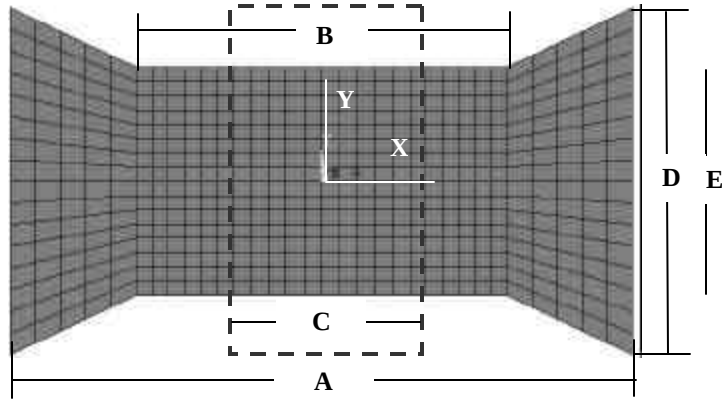

Fig. 3. Mesh of the switch membrane with dimensions A=320 μm, B=190 μm, C= 90 μm, D= 180 μm, and E= 100 μm, as used in the simulation. The membrane thickness is 300 nm, and the gap between the membrane and the bottom electrode is 4 μm. The dashed-line box shows the bottom electrode, whose width is equal to the switch edge width.

4.1. Effects of Residual Stress

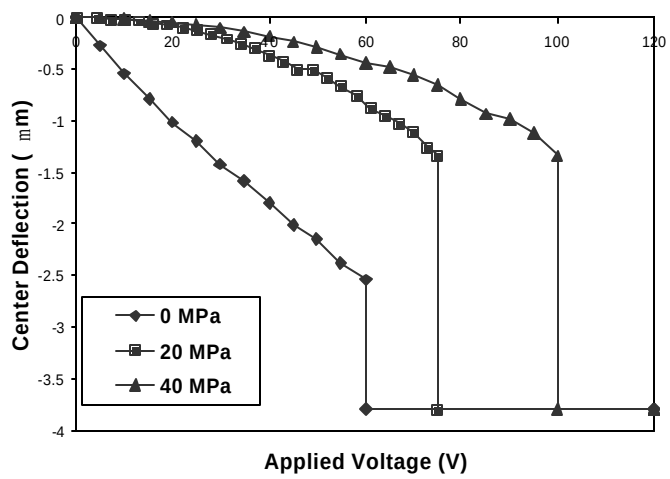

Fig. 4. Center deflection-applied voltage curves of a bow tie shaped flat switch with and without residual stresses.

We only consider the effect of tensile residual stresses. The tensile stress in RF switches usually ranges from a few MPa to over one hundred MPa [12-13]. 20 MPa and 40 MPa tensile stresses were applied to the bow tie shaped switch to examine its effect on pull-in voltage. The center deflection-applied voltage curves predicted by the analyses are shown in Fig. 4. It can be seen that the tensile residual stress increases the pull-in voltage and that values in excess of 100 V are needed when the residual stress is 40 MPa. It is known that actuation voltages this high typically result in switch failure after a limited number of actuation cycles. The failure occurs because of charge build-up in the dielectric layer [14].

4.2. Effects of initial stress

Sswitch membrane out-of-plane profiles were obtained by certain microfabrication processes [15-16]. Such a profile affects the thermo-electro-mechanical performance of the

switch significantly. Two arbitrary profiles were examined in addition to the flat membrane (Fig. 5(a)). It can be seen that out-of-plane profile reduces the pull-in voltage dramatically, especially in the case of profile B. In these analyses, a zero state of residual stress was considered.

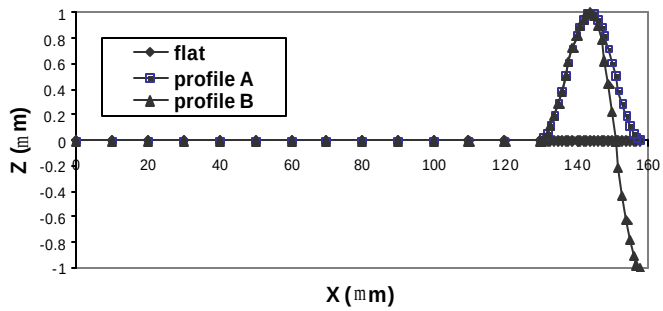

(a)

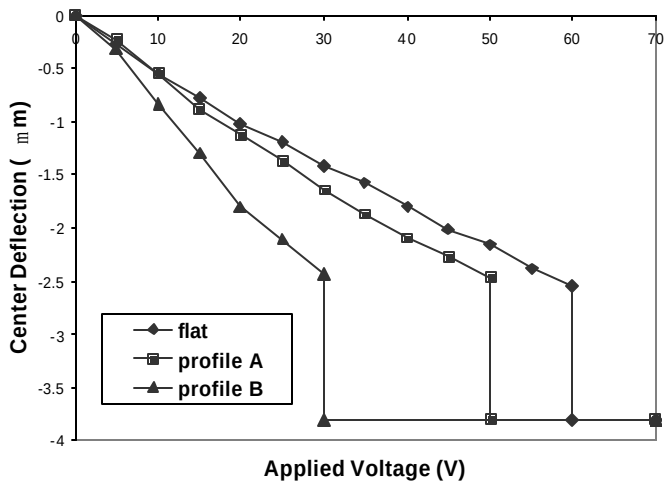

(b)

Fig. 5. (a) Out-of-plane profiles in addition to flat surface used to examine switch performance. Due to symmetry only half of the profile is shown. (b) Comparison of center deflection-applied voltage curves for flat surface and profiles A and B.

4.3. Effects of Temperature

Airplane condition monitoring and satellite wireless communication applications require the switches to perform at temperatures as low as –50°C [2-3]. The effects of operational temperature on switch behavior are shown in Fig. 6 for flat surface. It is observed that a temperature reduction from room temperature dramatically increases the pull-in voltage.

For a flat membrane, there is no out-of-plane profile change because the membrane develops tensile stresses when temperature is reduced. Moreover, the average value of the von Mises stress in the constant width region reaches a value of about 70 MPa, while that close to the supports reduces to about 50 MPa, as shown in Fig. 7. This thermal stress state increases the pull-in voltage, as we see from the effects of residual stress. For the switch with wavy profiles, temperature also alters the out-of-plane profile, which in turn affects the pull-in voltage, see [10] for details.

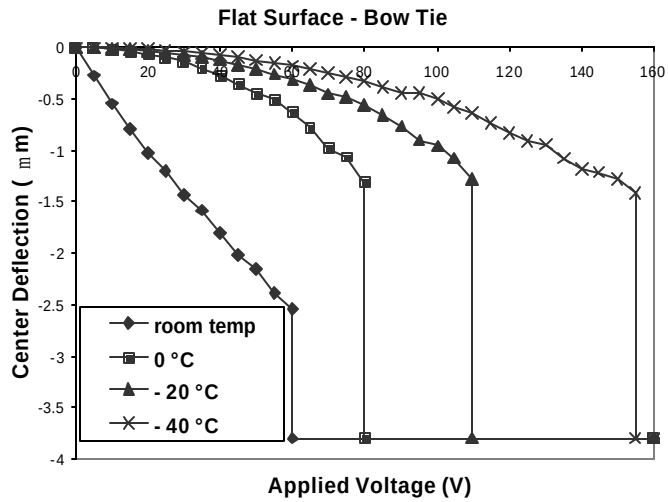

Fig. 6. Center deflection-applied voltage curves for a bow tie shaped flat switch at different operational temperatures. Room temperature refers to 20 ^{o}C here.

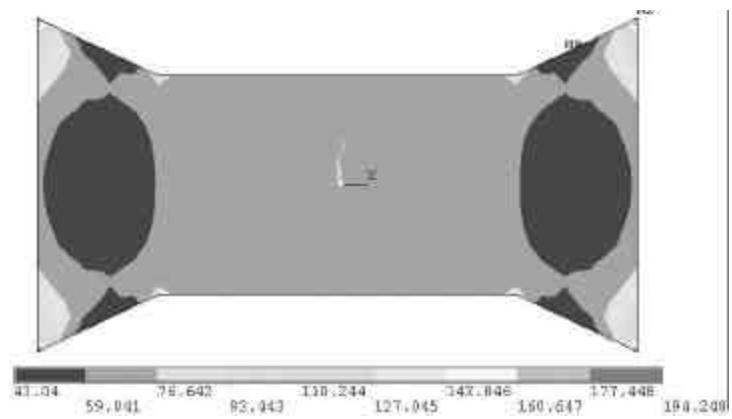

Fig. 7. Contours of von Mises stress for flat membrane at -20 ^{o}C before actuation.

5. CONCLUSIONS

A major obstacle in the commercialization of RF MEMS switches is their reliability. Mechanical modeling is an important tool for performance optimization and device reliability. 1-D, 2-D, and 3-D analytical models including nonlinear kinematics, which are appropriate for the MEMS switches, are developed in this paper. These models can accurately describe any types of MEMS devices with arbitrary in-plane shape and residual stress. However, in the case of out-of-plane profile and various temperatures, 3-D Finite Element Analysis (FEA) model has to be employed. This paper develops a 3-D FEA model including electrostatic, structural, and thermal domains using ANSYS/Multiphysis. Some of the results of a bow-tie shaped capacitive coupling switch are presented. This complete set of models including various analytical models and FEA model provide a powerful tool for the development of MEMS devices, in particular, RF MEMS switches at various operational temperatures.

REFERENCES

1. Rebeiz, G. M., RF MEMS: theory, design and technology, John Wiley & Sons, Hoboken, NJ (2003).
2. FAA 2nd Joint Annual COE Meeting, http://www.coe.faa.gov/proceedings/aace_docs/An%20Investigation%20of%20RF-MEMS%20Switches.pdf.
3. http://www.vs.afrl.af.mil/factsheets/TechSat21.html.
4. Z. J. Yao, S. Chen, S. Eshelman, D. Denniston and C. L. Goldsmith, Micromechined low-loss microwave switches, *J. Microelectromech. Syst*., **8** (1999) 129-134.
5. W. M. van Spengen, R. Puers, R. Mertens and I. De Wolf, A low frequency electrical test set-up for the reliability assessment of capacitive RF MEMS switches, *J. Micromech. Microeng*. **13** (2003) 604-612.
6. P. M. Osterberg and S. D. Senturia, M-test: a test chip for MEMS material property measurement using electrostatically actuated test structures, *J. Microelectromech. Syst*., **6** (1997) 107-118.
7. E. S. Hung and S. D. Senturia, Extending the travel range of analog-tuned electrostatic actuators, *J. Microelectromech. Syst*., **8** (1999) 497-505.
8. P. L. Gould, Analysis of shells and plates, Springer-Verlag, New York (1998) p. 358.
9. R. W. Hamming, Numerical methods for scientists and engineers, McGraw-Hill, New York (1973).
10. Y. Zhu and H. D. Espinosa, Effect of temperature on capacitive RF MEMS switch reliability – a coupled-field analysis, submitted to *J. Micromech. Microeng*., 2003.
11. V. L. Rabinov, R. J. Gupta and S. D. Senturia, The effect of release etch-holes on the electromechanical behavior of MEMS structures, in *Tech. Digest, 1997 Int. Conf. on Solid-State Sensors and Actuators*, 1997, pp. 1125-1128.
12. S. Chen, T. V. Baughn, Z. J. Yao, C. L. Goldsmith, A new in-situ residual stress measurement method for a MEMS thin fixed-fixed beam structure, *J. Microelectromechan. Syst*., **11** (2002) 309-316.
13. H. D. Espinosa, Y. Zhu, M. Fischer and J. Hutchison, An experimental/computational approach to identify moduli and residual stress in MEMS RF-switches, *Experimental Mechanics*, in press 2003.
14. C. Goldsmith, J. Ehmke, A. Malczewski, B. Pollans, S. Eschelman, Z. Yao, J. Brank and M. Eberly, Life time characterization of capacitive RF MEMS switches, in *IEEE MTT-S International Microwave Symposium*, Phoenix, Arizona, May 2001, pp. 227-230.
15. X. Chauffleur, L. Rabbia, P. Pons, K. Grenier, R. Plana and L. Dantas, Effect of membrane shape on mechanical behavior of RF switches, in *Tech. Digest, 16th Euro. Conf. on Solid-State Transducers*, 2002, pp 92-95.
16. G-L. Tan and G. M. Rebeiz, A DC-contact MEMS shunt switch, *IEEE Microwave and Wireless Components Letters* **12** (2002) 212-214.